Final Report for the Office of Hydrologic Development
NATIONAL OCEANIC AND ATMOSPHERIC ADMINISTRATION
NATIONAL WEATHER SERVICE

Project title

**VERTICAL PROFILE OF REFLECTIVITY AND BEAM OCCULTATION
STUDIES FOR IMPROVED RADAR-RAINFALL ESTIMATION**

NOAA Grant:
NA17WH1386

Principal Investigator:

Witold F. Krajewski
IIHR-Hydroscience & Engineering
The University of Iowa
Iowa City, Iowa 52242
witold-krajewski@uiowa.edu

Report Authors:

Witold F. Krajewski and Paul Kucera

October 2002

Introduction

We developed and tested the GIS-based software for radar beam propagation using our database for Guam. We have collected there a long data set of radar reflectivity (Level II) data. We also have a high-resolution (10 m) digital elevation data for Guam.

Guam is a 550 km^2 island centered at approximately 13°25'N, 144°45'E in the western North Pacific (see Figure 1). It is a 50-km long, elongated-shaped, northeast-southwest oriented island about 18 km wide at the northern and southern ends and 6.4 km wide at the middle. The northern half of the island is a relatively flat, uplifted limestone plateau ranging in elevation from 80 m to 220 m. There are two significant hills on the plateau, Mount Santa Rosa and Mount Barrigada. The southern half of the island is composed of basaltic mountains and hills, with a maximum elevation of 406 m and with five peaks exceeding 330 m (1000 ft). For interested reader, a detailed description of the geological characteristics of Guam and surrounding islands is given by Ward et al. (1965).

Guam Weather Surveillance Radar

Weather radar data collected on Guam were recorded by an operational Weather Surveillance Radar - 1988 Doppler (WSR88D) radar, which is part of the U.S. Next Generation Weather Radar (NEXRAD) network (Heiss et al. 1990; Crum 1993, 1998). WSR88D radars transmit at a wavelength around 10 cm (frequency of 2.9 GHz). WSR88D radars transmit horizontally polarized electromagnetic radiation at a peak

power of 475 kW. WSR88D radars have a high-resolution half-power (3 dB) beamwidth of 1°. The pulse repetition frequency of the radar ranges from 320-1000 Hz for two fixed pulse widths of 1.57 and 4.5µs. Data are collected and stored in spherical coordinates (range, azimuth, elevation). The radar has a range resolution of 1 km and azimuth resolution of 1°.

The WSR88D radar on Guam (NWS identifier PGUA) is located on the east-central side of the island (see Figure 2). In was commissioned on 22 October 1992. The WSR88D radar is operated and maintained by Andersen Air Force Base (AAFB) personal. It collects three moments of the returned signal: radar reflectivity, mean Doppler velocity, and Doppler velocity spectral width. The Guam WSR88D radar data are recorded and stored in a raw product format called Level II Archive data. These products are digitally stored to 8 mm magnetic tapes and sent to the National Climatology Data Center (NCDC). We have obtained the Level II data by two avenues. First, we obtained all Guam data that existed at NCDC through an agreement with the NASA Tropical Rainfall Measuring Mission (TRMM) office. After TRMM was launched, AAFB weather office personal in collaboration with the University of Guam made copies of the archive tapes at the site and sent them to the University of Iowa. To provide fast, efficient access to the entire data set, radar reflectivity data are stored online in an ASCII Run-Length Encoded (RLE) that was designed for radar data and described by Kruger and Krajewski (1997).

This study encompasses Guam WSR88D data collected between December 1997 and August 2000. Guam has numerous problems that require various quality control and

masking algorithms to exclude compromised WSR88D radar data from ground validation analysis. We processed all the radar volumes scans between 1995 and 2000 to examine the long term spatial patterns of observed reflectivity to see what sectors might be usable for analysis. One interesting derived field that can be calculated from the radar reflectivity is the probability of detection (POD). Using the POD over a long period, regions of sea clutter, ground clutter, and beam blockage are easily detectable and identified. To understand the significance of the POD maps, radar data is compared with a radar beam propagation model. The model incorporates USGS digital elevation model (DEM) to compare the correspondence of the ground clutter and beam blocked sectors with location of terrain features. Using the POD and model results, a product map can be created to exclude regions where the full signal from meteorological echo cannot be obtained.

Reflectivity Probability of Detection (POD) Maps

We calculated the POD for all the sweeps recorded in a radar volume. Figure 3 shows the radar reflectivity POD out to a maximum range of 150 km for the lowest two sweeps. Data from all the collected radar volumes were used in the analysis for the period May 1995 – August 2000. There is about 125,000 volume scans available during this period. The POD units are in percentage observations that occurred above a reflectivity threshold of 10 dBZ. We chose a 10 dBZ threshold because it represents the nominal reflectivity that would be considered detectable surface rainfall (~ 0.1 mm h^{-1}) and it reduces contamination from sea clutter.

There are several features in the lowest elevation POD field worth noting. Even though the threshold reduces sea clutter signature, its signature is still observed in the POD map. It is the feature that has a relative high POD (> 18 %) within the first 30 km east and to a lesser extent to the NNW of Guam. A second feature that is prominent is the high POD associated with the mountainous regions (ground clutter) throughout the island. The locations of the high POD on the island correspond to the mountains on Guam. Behind the mountainous regions is the relatively small POD due to the beam blockage. Severe blockage (close to 100 %) is seen for a sector between azimuths 16° and 30°, which corresponds to the direction of Rota. A lesser amount of beam blockage is detected to an azimuth of 68°. There is also significant blockage from the mountains to the SW. The blocked sector encompasses a region bounded by azimuths 212° and 281°. The last main feature is the entire blockage in a four-degree sector to the S (187° – 192°). The sector is blocked because of an apartment complex (Ladera Towers), which was built after the radar was installed is located within 1 km of the radar. It is interesting to note that the POD in unblocked sectors without significant clutter has a mean POD of about 8 %. If one assumes that all the return detected is from meteorological echo (i.e. rainfall), the Guam region observes rainfall about 8 % of the time.

Radar Beam Propagation Model Results

To asses the severity of the blockage and to create a product map for validation comparisons, we developed a radar beam propagation model that incorporates DEM data. The model calculates the relative power loss as function range, elevation, and azimuth of the radar beam as it interacts with the terrain features stored in the DEM data. The USGS has published a DEM manual (USGS 2000) that gives detailed description of the

different model resolutions, DEM data collection methods, data characteristics for various regions around the world, format of the data records, and the accuracy of the DEM data. The horizontal resolution of Guam DEM data is 10 m, which is relatively high in comparison to most DEM datasets (30 m resolution). Data accuracy is reported to be one-half a contour interval or better which corresponds to < 5 m. Using resampling of the 10 m resolution data we also investigated the effect of using the 30 m and the 100 m resolution DEM data.

The beam propagation model assumes standard refractive atmosphere (Battan 1973) to calculate the height of the beam as function of range. The height of the beam can be estimated by the following equation (Rinehart 1991):

$$h = \sqrt{r^2 + R'^2 + 2rR'\sin(\theta_e)} - R' + h_0, \qquad (1)$$

where h is the height above the radar, r is the slant range from the radar, R' is the effective Earth's radius to account for atmospheric refraction, θ_e is the elevation angle of the radar beam, h_0 is the height of the antenna above a reference point (above ground, above mean sea level, etc.). The effective radius, R', can be estimated by assuming the change in refractive index with height in the lower atmosphere is constant. With this assumption, R' is approximately 8500 km. The standard refractive atmosphere assumption will be evaluated in further sections.

The model also assumes that surface features (trees, buildings, etc.) that are not represented in the DEM model do not contribute significantly to the scattering of the

radar beam power. If the surface features in the vicinity of the radar were known accurately, characteristic roughness lengths could be determined and incorporated into the model. This idea was not explored in my dissertation but could be added as future research.

I also assumed that when a portion of the beam was lower than the terrain, the power in the portion of the beam below the surface height was scattered back (ground clutter), absorbed by the surface, or scattered in direction perpendicular to the path of the beam and no power was scattered in the forward direction. In reality, some of the power would also be scattered forward and contribute to received power beyond the beam blockage. Because of the complexity of the interaction of electromagnetic waves with terrain, this amount of forward scattered power would is unknown and therefore was not considered in my model.

To evaluate the integral of power within a beam, a common approximation is to assume that the distribution of power within the main lobe can be represented by a two dimensional Gaussian illumination function (Probert-Jones 1962; Donaldson 1964; Meneghini and Kozu 1990), which is given by the following equation:

$$f(\theta,\phi) = \exp\left\{-\ln 2\left[\left(2\frac{\theta}{\theta_3}\right)^2 + \left(2\frac{\phi}{\phi_3}\right)^2\right]\right\}, \tag{2}$$

where θ_3 and ϕ_3 are the half-power or 3 dB beamwidths along the principal axes (defined to be the angular distance across the main lobe where the power is reduced by one half of the peak power at the point of maximum gain, $f(\theta,\phi) = 0.5$). The azimuth

angles θ and ϕ are measured from the point of maximum gain. The factor of two is multiplied to the azimuth angles to account for the angles are only half the total angular distance across the beam. If the antenna is symmetric (i.e. a circular beam), which is the case for WSR88D radars, the Gaussian illumination function can be simplified to:

$$f(\theta) = \exp\left[-\ln 2\left(2\frac{\theta}{\theta_3}\right)^2\right], \tag{3}$$

where θ is the polar angle measured from the point of maximum gain.

In the model, sidelobes are neglected. The error in ignoring sidelobe can become significant in special circumstances when strong reflectivity gradients are present within the beam volume. For example, the region near the melting often has a strong gradient of reflectivity, which can cause significant sidelobe effects. On the other hand, this is normally not a problem except at far ranges for rainfall estimation algorithms because the lowest tilts are commonly used which remain below the melting level. In general, a Gaussian beam pattern approximation is a good assumption when measured power in the sidelobes is significantly smaller then the main lobe. The first sidelobe for WSR88D radars is reported to be -27 dB down (Doviak and Zrnić 1993), which about 500 times smaller than the main lobe power.

Probert-Jones (1962) compared the Gaussian beam approximation to a well-known class of antenna beam patterns that use complicated Bessel functions to represent both the main lobe and sidelobes. He found the Gaussian approximation for more complicated beam patterns varies less than 0.64 dB in comparison in most cases. Other investigators

have also shown the Gaussian beam pattern is a good approximation for most meteorological applications (Donaldson 1964; Bogush 1989; Andrieu and Creutin 1995).

The Gaussian beam pattern was extended to a 6 dB beamwidth in our model. This will capture 93.75% of the total power with the assumed beam pattern. The beam pattern in the plane perpendicular to the propagation path was divided into small $0.1° \times 0.1°$ elements to capture the fine scale interactions with the DEM data. A total of 3×10^5 elements are used in the integration of beam power. The power in each element is weighted Gaussian illumination function such that when all the elements are integrated over the entire beam pattern, the following relationship is satisfied:

$$p_t = \int_0^{\theta_6} \int_0^{2\pi} f^2(\theta) d^2 p_s(\alpha,\theta) \theta d\theta d\alpha = 1, \tag{4}$$

where p_t is the total normalized power. The function $f^2(\theta)$ is the two-dimensional normalized form of equation (3), $d^2 p_s(\alpha,\theta)$ is the power in each elemental unit, s, and θ_6 represents the integration over the 6 dB beamwidth.

To examine the beam blockage as a function of azimuth and range from the radar, the DEM data were resampled into 0.1° azimuth × 0.1 km range bins. The bins extended to a maximum range of 30 km from the Guam radar. In other words, for every 0.1° in azimuth, there were 300 ranges bins for a total of 1.08×10^6 resampled DEM data bins over the 360° azimuth angles.

For every 0.1° in azimuth, the relative power remaining in the beam is calculated. At every range bin, the power would be integrated over the 6 dB beam pattern. If any of the

power elements in the beam intersected or fell below the land surface, the power in those elements would be subtracted from the total power available. Once blocked, the power in those elements would no longer contribute to the total power downrange. The power loss is then integrated as function of range to obtain a total power for a particular azimuth angle. Mathematically, the power loss at each range can be written:

$$p_i = \int_0^{\theta_u}\int_0^{2\pi} f^2(\theta)d^2 p_s(\alpha,\theta)\theta d\theta d\alpha <= 1, \tag{5}$$

where p_i is the power loss at the ith range bin, θ_u is the polar angle subtended from the center of the beam to the point where beam remains unblocked for a azimuth angle, α, in the beam pattern. Obviously, this would be the 6 dB half beamwidth ($\theta_u = \theta_6$) if there is no beam blockage. At each range bin, the relative power loss can be calculated by the following equation:

$$p_{loss_i} = \frac{p_i}{p_t}, \tag{6}$$

or the power loss can be examined in logarithmic units:

$$p_{loss_i}(dB) = 10\log(p_{loss_i}) = 10\log\left(\frac{p_i}{p_t}\right). \tag{7}$$

Because $p_i \leq p_t$, the relative power loss will be ≤ 0 dB. The total power loss along an azimuth equals the power loss at the maximum range of the DEM data. In my study, the maximum range is 30 km and the DEM bins are spaced 0.1 km. Therefore, the total power loss is: $p_{loss_{total}} = p_{loss_{300}}$.

Several steps were implemented to determine with elements in the beam pattern were blocked by the terrain. The first step was to determine the relative height difference of the center of the beam to the ground. The height of the antenna is 30 m above ground level (AGL) and base of the antenna tower is located 80.5 m above mean sea level (MSL). At each range bin, the height of the center of the beam is estimated using equation (1). The next is to calculate the height of each elemental bin in the beam pattern using the center beam height as a reference. The height above MSL is then easily calculated for each beam pattern bin. The location in relation to the ground for each element in the beam pattern is also calculated knowing the range and azimuth of the center of the beam.

The height of each beam element is then compared to the DEM data at that location. To provide a better comparison in heights, a cubic spline interpolation was fit to the DEM data in the azimuth directions at each range using the algorithm developed by Press et al. (1992). This provided good estimates of the land height in the regions between the discrete DEM data points. If the beam pattern element was located at the same height or below the elevation of the land, it was flagged as blocked. After all (if any) blocked beam elements are located, the total power was calculated using all the non-blocked beam elements. As we stated earlier, once a beam element is considered blocked, it remains flagged as blocked for the remainder of the propagation path. The beam is examined for additional blockage at the next range step and the power loss is recalculated. This procedure repeated along the range to obtain the total power loss along that azimuth

angle. The algorithm is then applied to all the azimuth angles to obtain two dimensional power loss map and total power loss estimate as function of azimuth angle from the radar. These steps are then repeated for each elevation sweep until no blockage is detected.

The total power loss for the lowest two sweeps is show in Figure 4. In the first sweep, over 50 % of the sectors have at least partial blockage. The beam blockage is corresponds to locations with lower POD due to beam blockage shown in Figure 3. Two main blockages are detected with the model. The first blockage is between azimuths 355° − 75°. The second blocked sector is to the SW between azimuths 200° and 285°. The second analysis shows very little beam blockage except for partial beam blockage (~0.7 dB) in the direction of Rota. In Figure 5 we show the same results but all three resolutions we investigated. In this view little differences show up between the different resolutions. Only when we plot the relative power loss the differences become more apparent (Figure 6).

It is important to see if the location of the beam blockage varies with radar observations. For this analysis, we plotted the POD and two dimensional power loss maps on the same Cartesian coordinate system. The resolution of the grid is 4 km to match the resolution HRAP grid. The two dimensional DEM blockage maps are shown for the lowest two elevation sweeps in Figure 7 (recall the POD maps are shown in Figure 3). The power loss is given in positive dB (the negative sign has been dropped for display purposes). It is important to see if the model agrees with the long-term observation.

The spatial patterns of beam blockage and POD agree quite well. The significant blockages are located along the same azimuths. Some of the weaker beam blockage that is indicated in the DEM model is not prominently seen in the POD. For example, the

weak blockage in azimuths 355°–15° is not detected in the POD map. Also, the weak blocked sector to the SW (200°–210°) is not a feature detected in the POD analysis. The second sweep results also agree well. Both show very little blockage except for a small amount in the direction of the Rota Island.

The last comparison that we performed was to see if a relationship could be formed between power loss estimated by my beam propagation model and the long term POD using radar reflectivity data. For this analysis, we compared the total power loss to the POD of detection at 1 azimuth angles. The power loss was used was taken at the range of maximum loss (just beyond the maximum distance of the island). The representative POD was extracted at range that was outside the range of sea and ground clutter as but close enough that range effects was not an issue. From the two-dimensional map, a range of 50 km met the criteria for a representative sample. The scatter plot of the comparison is shown in Figure 8. Clearly, there is a strong relationship between DEM power loss and the decrease in the POD. The points located along ordinate axis indicate the regions of no beam blockage. The range of values represents the natural variability in POD observed near Guam. The last step was to fit a regression model to the data. We compared several models and the determined that quadratic model gave the best fit. The model has the following form:

$$POD = -0.0059P_{loss}^2 - 0.3086P + 7.642, \tag{8}$$

where P_{loss} is the power loss derived from the DEM data. All the points with 0 dB power loss were excluded from the analysis. The adjusted R^2 value for the model was 0.9469 with a RMSE of 0.4776.

The same analysis performed for lower resolution DEM data shows that actually the best agreement between the POD maps and the beam propagation model is for the high resolution data (Figure 9). Decreasing the resolution increases the scatter between the two quantities. Based on our study, long term POD can be a good predictor of regions with power loss or blocked sectors. This information can be used to flag sectors that should be excluded from further analysis.

We used the combination of DEM beam blockage model and POD results to create a product map for Guam. The map accounts for blockage in the first and second sweeps. We took a conservative approach in that we make no attempt to estimate reflectivity in blocked sectors. Before we made this decision, we tested a vertical profile of reflectivity (VPR) developed by Vignal et al. (1999), Vignal et al. (2000) and Vignal and Krajewski (2001) in a unblocked sector to see if reflectivity information in the upper tilts contained enough information to recover the lowest sweep data. The results of this study (not shown) indicate that the VPR estimate could be a factor of 10 off from the "true" value in the lowest sweep. The model was designed to work well in fairly uniform precipitation such as stratiform rainfall. We believe the shallow, convective nature of the precipitation features observed on Guam was the main factor in the VPR retrieval.

Atmospheric sounding data were also analyzed to examine the characteristics of the atmosphere during different climatological conditions and examine the sensitivity of using the standard refraction for the radar beam propagation. Sounding data for the years of 1997–2000 were obtained from database by the Atmospheric Science Department at the University of Wyoming (http://weather.uwyo.edu/upperair/sounding.html). Nominally, soundings are launched every 12 hours (synoptic period) at 00 and 12 UTC.

Non Standard Refraction Beam Height

The exact formulation for the propagation of electromagnetic beam is given by the following equation:

$$s(h) = \int_0^h \frac{RCdh}{r[r^2 n^2(h) - C^2]^{1/2}} ,$$

$$C = Rn(0)\cos(\theta_e)$$

(9)

where $s(h)$ is the distance along the Earth's surface to a point directly below the ray at height h, R is the Earth's radius, r is the distance from the center of the Earth to the location of the ray $(R + h)$, θ_e is the elevation angle above the horizon, and $n(0)$ is the refractive index at the surface (at the radar). The main assumption is that the refractive index is smoothly changing for a given wavelength such that ray theory applies. It can be shown that equation (9) is the exact solution to the second order differential equation (Hartree et al. 1946):

$$\frac{d^2 h}{ds^2} - \left(\frac{2}{r} + \frac{1}{n}\frac{dn}{dh}\right)\left(\frac{dh}{ds}\right)^2 - \left(\frac{r}{R}\right)^2 \left(\frac{1}{r} + \frac{1}{n}\frac{dn}{dh}\right) = 0 .$$

(10)

It can be shown that equation (10) can be solved to obtain an Earth equivalent model by assuming a standard refractive atmosphere. There are times when this assumption does not hold (i.e. inversions, frontal boundaries, etc.). We wanted to examine the

sensitivity of using a 4/3rd Earth approximation in our beam occultation analysis. This can be done if we assume a spherically stratified atmosphere and the refractive index can be represented by a piecewise linear model of n verses h. In this case, equation (10) can be linearized with respect to h to determine the radar beam location as a function of height which results in the following equation:

$$s(h) = \left[\frac{\cos\theta_e}{1 + \beta_0 R} \right] \left\{ [R^2 \sin^2\theta_e + 2R(1 + \beta_0 R)h]^{1/2} - R\sin\theta_e \right\}, \qquad (11)$$

where β_0 is the gradient of n at the surface (Doviak and Zrnić 1993). Because $n(0)$ is near unity and much smaller than R in equation (11), we have substituted 1 for $n(0)$. The ray location at the next height step can be determined by using equation (11) and modifying it to reflect the condition at the boundary between the two refractive layers:

$$s'(h') = \left[\frac{\cos\theta'_e}{1 + \beta_1 R'} \right] \left\{ [R'^2 \sin^2\theta'_e + 2R'(1 + \beta_1 R')h']^{1/2} - R'\sin\theta'_e \right\}, \qquad (12)$$

where $s'(h')$ is ground distance from the point of emergence of the ray from the layer below, h' is the height of the ray above the top of the previous layer h_1, $R' = R + h_1$, and θ'_e is the angle made from the ray at height h_1. The angle, θ'_e, can be calculated by the following equation:

$$\theta'_e = \tan^{-1}\left\{\left[R^2\sin^2\theta_e + 2Rh_1(1+\beta_0 R)\right]^{1/2} / R\cos\theta_e\right\}. \tag{13}$$

The piecewise linear steps can be repeated until the gradient becomes constant or the maximum range from the radar is reached. To examine the assumption of the 4/3rd Earth ray propagation model, atmospheric soundings were used to obtain the state of the atmosphere over Guam. For our study, we used over 2000 soundings that were recorded between December 1997 and August 2000.

The results of using the ray propagations given above for these soundings are given in Figure 10. The estimated height-distance relationships from the observed refraction profiles are indicated by thin gray lines. The mean profile along with +/- one standard deviation is plotted in 25 km intervals. As a reference, the 4/3rd Earth model is plotted as black line. The total variation in height from the Earth equivalent model is on the order of 10 m for distances less than 25 km. At the maximum range of 150 km, the estimated beam heights ranged from 2 km to 3 km (excluding the bottom outlier), indicating that the 4/3rd Earth model could off by 500 m in height at this range.

In most cases, the agreement between the estimated beam height and the 4/3rd Earth model is much better. At all distances, the mean height lies close to the 4/3rd Earth line. The plot shows the mean values slightly higher than the standard beam propagation model. The difference ranged from 10 m to 49 m for distances of 25 km and 125 km, respectively. The standard deviation about the mean was 8.1 m at 25 km and 99 m at 125 km. The standard refraction beam height estimate was always within one standard deviation of the actual sounding estimates and was less than 50 m from the mean for all distance values.

Except for a few percent of the cases, the 4/3rd Earth beam height approximation is good assumption of Guam. Variations in actual beam heights is very sensitive to large gradients of refraction due to temperature inversions and vertical gradients of water vapor in the lowest layer of the atmosphere (~100 m) (Doviak and Zrnić 1993). Guam has at least two factors minimizing anomalous beam propagation. First, we observed few level temperature inversions. The ocean sea surface temperature is warm and relatively constant throughout the diurnal cycle, counter acting any radiation cooling in the boundary layer. Generally, the inversions occurred 2-4 km AGL. At this height, a radar beam is propagating through the varying layers at angles that are insensitive to changes in refraction. Second, the radar is located ~100 m above the ocean surface so the beam is already above the height where most of the large variations are observed. On the other hand, the atmospheric profile of temperature and moisture has a relatively course resolution using standard rawindsonde data. The instrumentation is not designed to have a fast time response to capture large variations in thin vertical layers. Therefore, our results are probably an optimistic view of the variability of beam propagation with range. High resolution data from aircraft or lidar observations would be necessary to improve the beam propagation model.

To test the sensitivity of actual height calculations, we implemented the estimated beam heights shown in Figure 10 into the beam propagation-DEM interaction model. We tested the variation in beam power loss over the AAFB rain gauge site. The reason for this azimuth selection is because we wanted to determine the variability in beam blockage over the only high resolution, quality rain gauge installed on Guam and relatively unblocked by terrain. The results for this analysis are shown in Figure 11. This was performed for the first sweep only. Over the AAFB gauge site, the 4/3rd Earth estimated power loss due to beam blockage was 0.7 dB. We calculated the power loss

relative to the standard refraction model. The plot shows how the power loss increases as beam propagates over the terrain features stored in the DEM data. It is encouraging to see that most cases have a relative power loss within 5 % of the 4/3rd model. The power loss values greater than 5 % correspond to the outliers observed in Figure V.2. Based on our results, the 4/3rd Earth beam height approximation seems valid for most conditions observed on Guam.

Conclusions

The results indicate that using lower resolution DEM data can result in different estimates of power loss due to beam blockage, but it is not overly different except in more complex terrain. For Guam, the 100 m resolution comparison shows that change in power loss ranges from 2 dB to over -3.5 dB various azimuth angles. The 30 m resolution results show less variation. Two scenarios could result in less of a decrease (positive values in Fig. 6) or increase (negative values in Fig. 6) in power loss at the lower resolutions. For a decrease in power, the lower resolution data is not providing enough information about the finer scale structure in the terrain and therefore the blockage is likely to be less. Also, depending on where the 10 m DEM data were resampled, the representative point for the 100 m DEM cell could be in a relative elevation point, which would result in a lower power loss. On the hand, the resampled point could be located at higher location giving more power loss. Also, when the power loss is integrated at the higher height over longer downrange distances from the radar, it can result in more power loss due to the extended beam blockage. In any case, we think that the lower resolution data (especially the widely available 30 m data) can be used as a very useful tool to give estimates of possible blockage for existing sites and for

development of new radar site surveying. For detailed studies there is a new technology available, i.e. Airborne Laser Swath Mapping (ALSM) capable of providing data with resolution on the order of 1 m (Shrestha et al. 1999). For critical problems and location we recommend acquiring and such data for the beam propagation studies.

The comparison of the POD using Guam radar reflectivity observations shows that there is a strong relationship between the POD maps and power loss due to beam blockage. The results show more scatter for the lower resolution data but the main features of the POD map and power loss in the beam blocked regions are still clearly identified.

The product map derived from this study is shown in Figure 12. There are three main masked sectors. They correspond to the blocked region to the NE, the blocked region to the SW, and the blocked sector in the direction of the apartment building. The blocked sector over Rota in the second sweep is also flagged in the product map. The sector east of the severely blocked Rota sector is partially blocked in the lower sweep. Since for the further ranges we would have to use the lower sweeps in rainfall estimation, we decided to simply block that sector beyond about 70 km range. For closer ranges we can use the second sweep which is not blocked close to the radar. We used this map in all the analyses of rainfall estimation performance of the Tropical Rainfall Measuring Mission for NASA.

References

Andrieu, H. and J. D. Creutin, 1995: Identification of vertical profiles of radar reflectivity for hydrological applications using an inverse method. Part I. Formulation. *J. Appl. Meteor.*, 34, 225-239.

Battan, L. J., 1973: *Radar Observation of the Atmosphere*. The University of Chicago Press, 324 pp.

Bogush, A. J., 1989: *Radar and the Atmosphere*. Artech House, 452 pp.

Crum, T. D., R. E. Saffle, and J. W. Wilson, 1998: An update on the NEXRAD program and future WSR-88D support to operations. *Weather Forecasting*, **13**, 253-262.

Crum, T. D., R. L. Alberty, and D. W. Burgess, 1993: Recording, archiving and using WSR-88D data. *Bull. Amer. Meteor. Soc.*, **74**, 645-652.

Donaldson, R. J., Jr., 1964: A demonstration of antenna beam errors in radar reflectivity patterns. *J. Appl. Meteor.*, **3**, 611-623.

Doviak, R. J. and D. S. Zrnić, 1993: *Doppler Radar and Weather Observations, Academic Press*, San Diego, CA, 562 pp.

Hartree, D. R., Michel, J. G. L., and Nicolson, P., 1946: Practical methods for the solution of the equations of tropospheric refraction. Meteorological Factors in Radio Wave Propagation, Physical Society, 127-168.

Heiss, W. H., D. L. McGrew, and D. Sirmans, 1990: NEXRAD: Next Generation Weather Radar (WSR-88D). *Microwave J.*, **33**, 79-98.

Kruger, A. and W. F. Krajewski, 1997: Efficient storage of weather radar data. *Software Practice and Experience*, **27**, 623-635.

Meneghini, R. and T. Kozu, 1990: *Spaceborne Weather Radar*. Artech House, Inc., Norwood, MA, 199 pp.

Probert-Jones, J. R., 1962: The radar equation in meteorology. *Quart. J. Royal Meteor. Soc.*, **88**, 485-495.

Rinehart, R. E., 1991: *Radar for Meteorologists*, Available from R. E. Rinehart, Grand Forks, ND, 334 pp.

Shrestha, R.L., W.E. Carter, M. Lee, P. Finer and M. Sartori; 1999: Airborne Laser Swath Mapping: Accuracy Assessment for Surveying and Mapping Applications," *Journal of American Congress on Surveying and Mapping*, **59**(2), 83-94.

Vignal B., H. Andrieu, and J. D. Creutin, 1999: Identification of vertical profiles of reflectivity from volume scan radar data. *J. Appl. Meteor.*, **38**, 1214-1228.

Vignal B., G. Galli, J. Joss, and U. Germann, 2000: Test of different methods to determine vertical profiles of reflectivity and precipitation estimates from volumetric radar data. *J. Appl. Meteor.*, **39**, 1715-1726.

Vignal, B. and W.F. Krajewski, Large sample evaluation of two methods to correct range-dependent error for WSR-88D rainfall estimates, *Journal of Hydrometeorology*, **2**(5), 490-504, 2001.

Ward, P. E., S. H. Hoffard, and D. A. Davis, 1965: Hydrology of Guam. *Geological Survey Professional Paper 403-H*. Available from the US Government Printing Office, Washington, DC, 28 pp.
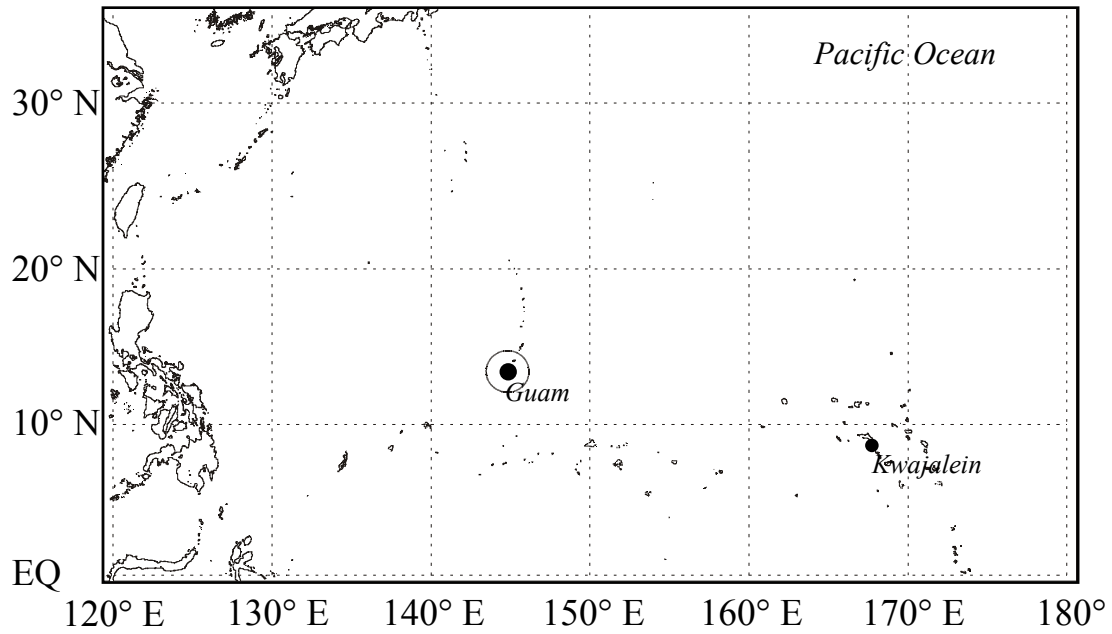
Figure 1: Map of the northern western Pacific Ocean basin. The boundaries of the map represent the maximum extent of the study area. The outer circle surrounding Guam shows the maximum coverage of the Guam radar.
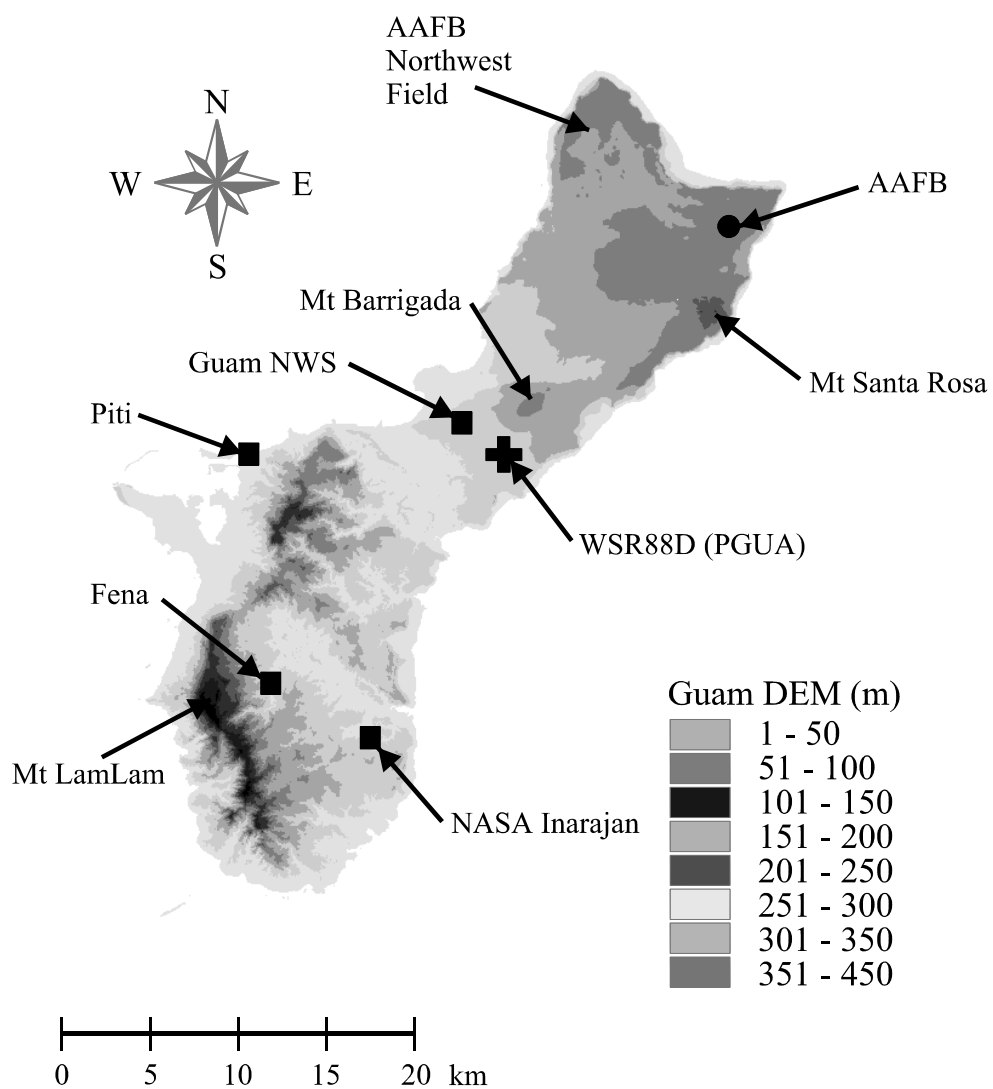
Figure 2: Elevation map of Guam showing the location of the WSR88D radar and rain gauges.
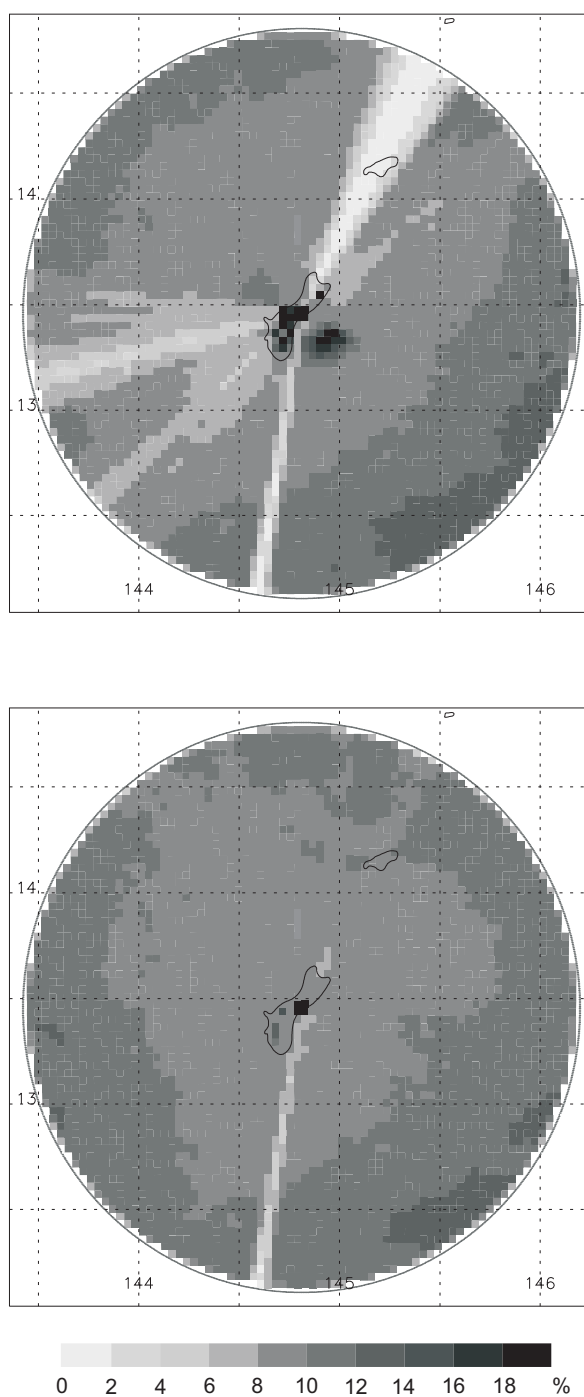
Figure 3: POD maps for the lowest two sweeps (0.5 and 1.5 elevation) for radar reflectivity using a threshold of 10 dBZ.
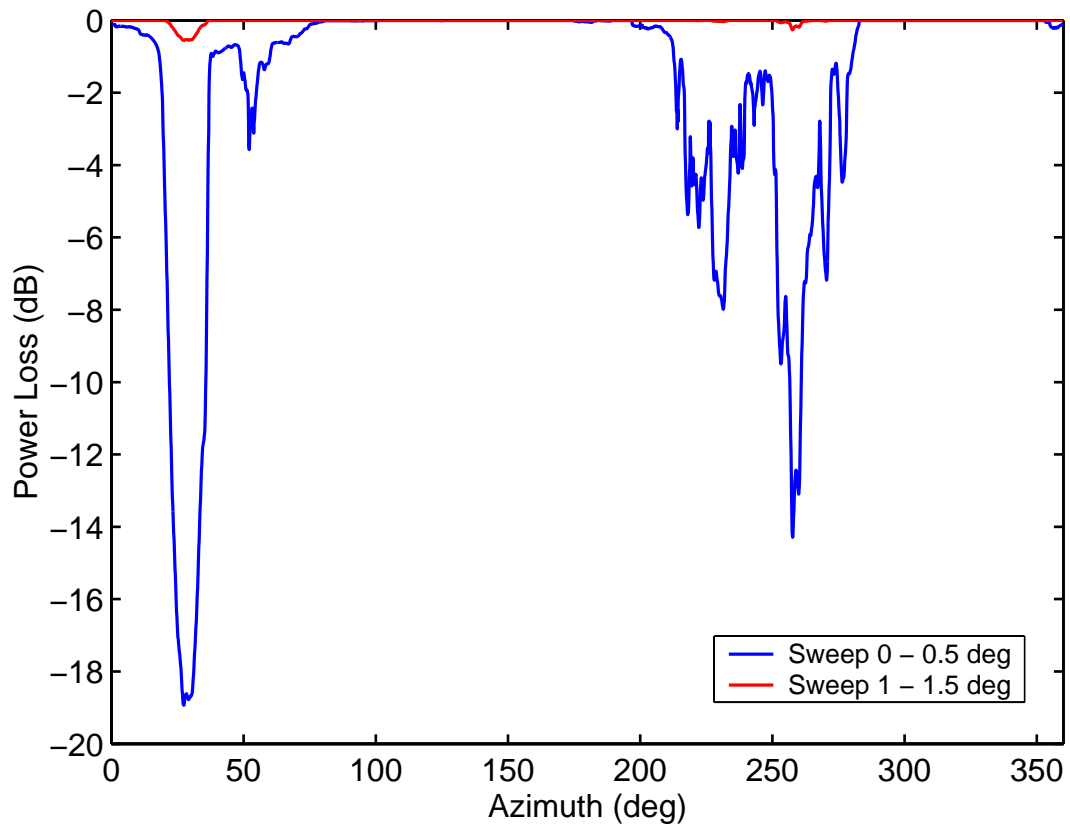
Figure 4: Estimated power loss due to beam blockage calculated from a beam propagation model and DEM data for the lowest two elevation sweeps.
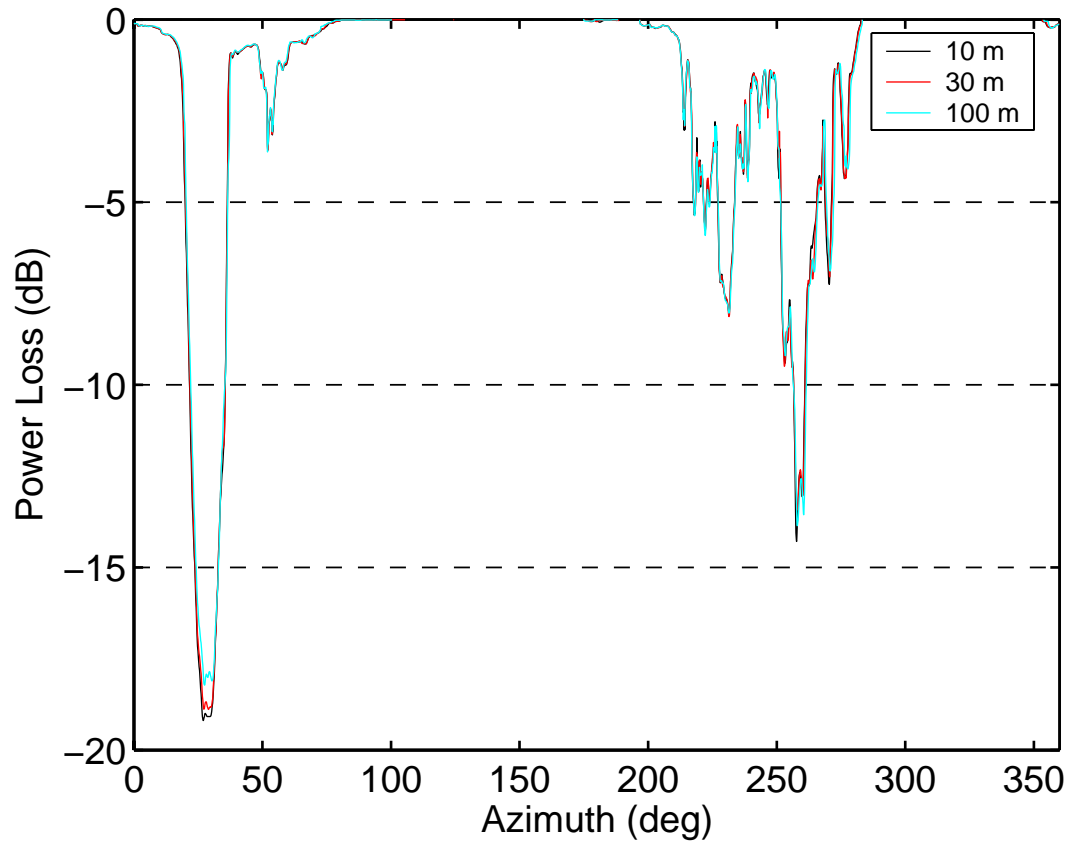
Figure 5: Estimated power loss due to beam blockage calculated with a beam propagation model and DEM data at resolutions of 10 m, 30 m, and 100 m. The original DEM data had a resolution of 10 m. They were resampled at 30 m and 100 m to simulate lower resolution data.
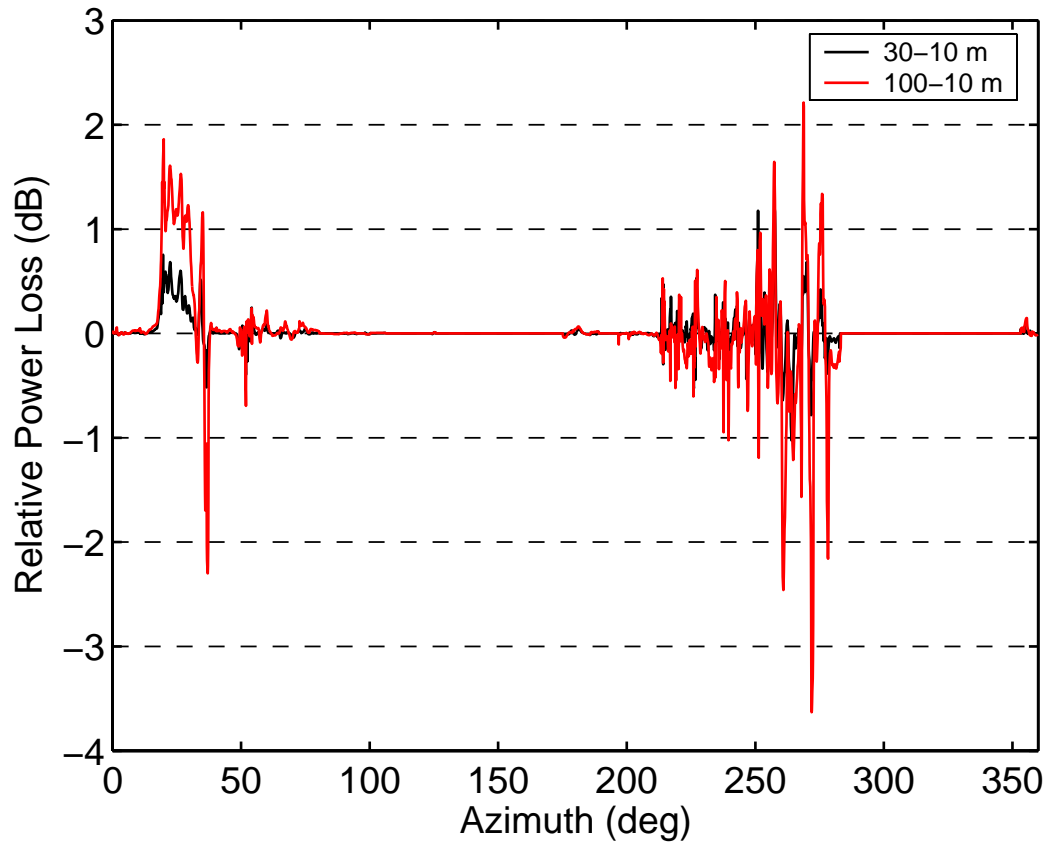
Figure 6: Relative power loss for the results shown in Fig. 5 of 30 m (black) and 100 m (red) compared to the power loss using 10 m DEM resolution. Positive values indicate lower resolution DEM data had a lower power loss compared to the 10 m DEM estimates.
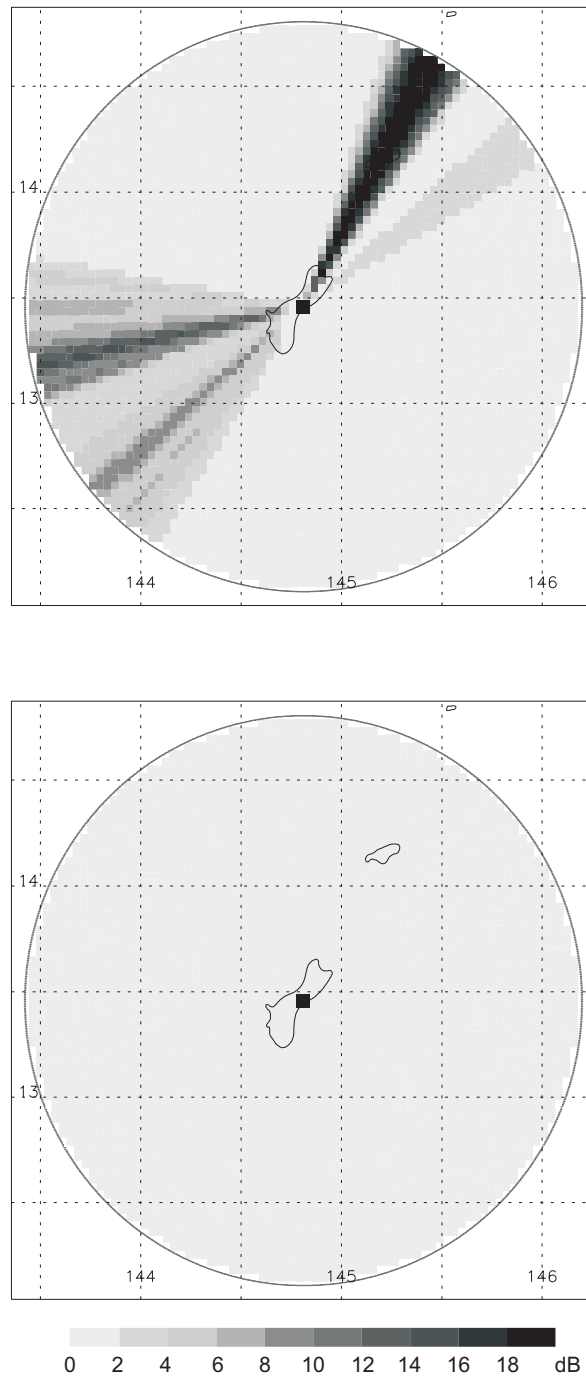
Figure 7: Two dimensional power loss maps derived from beam propagation model using DEM data. The top panel is the power loss map for the first elevation sweep (0.5°) and the bottom panel is for the second sweep (1.5°).
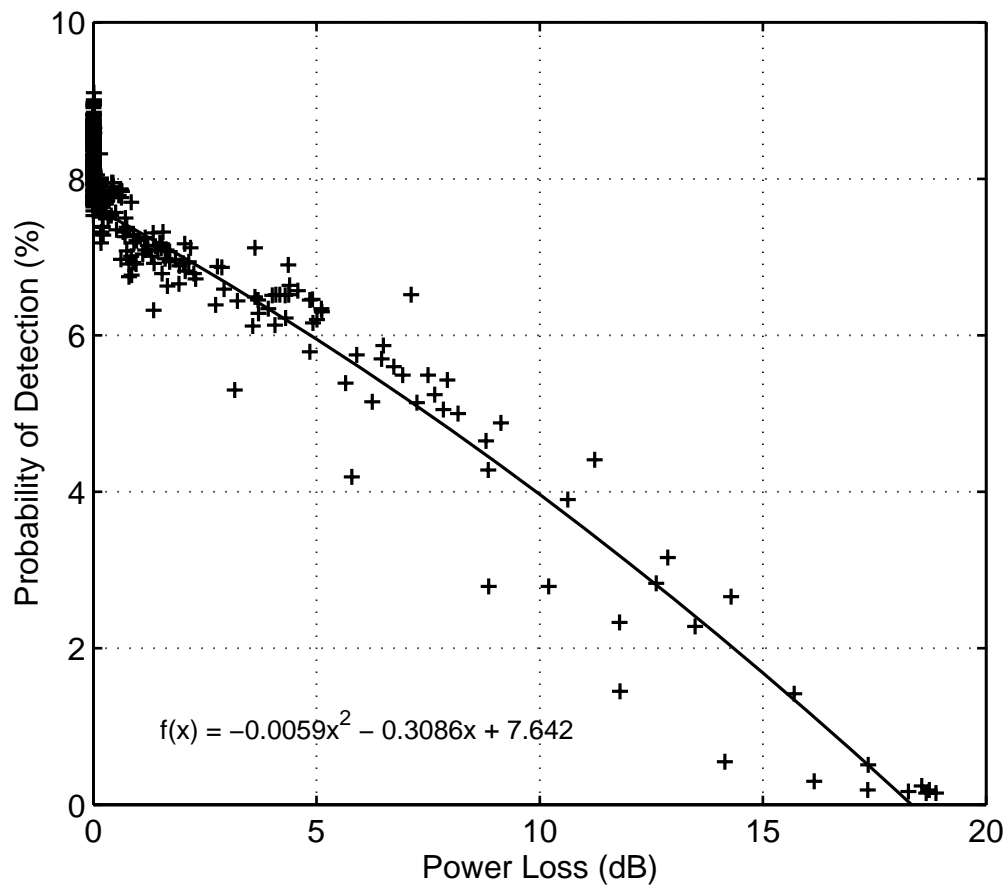
Figure 8: Scatter plot of POD verses power loss for 1° azimuth angles around Guam. The power loss was calculated from beam propagation model. The POD at a range of 50 km was used in the comparison.
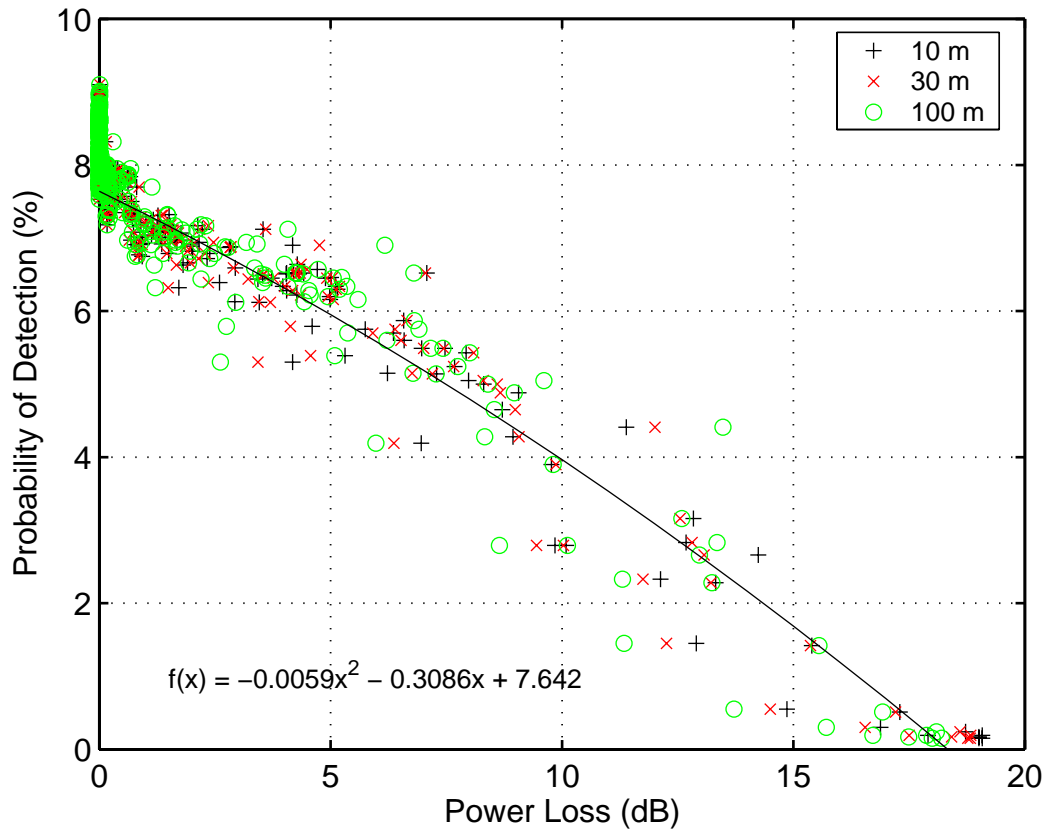
Figure 9: Scatter plot of probability of detection (POD) verses power loss for 1 azimuth angles around Guam. The power loss was calculated using a beam propagation model and DEM data at resolutions of 10 m, 30 m, and 100 m. The POD at a range of 50 km was used in the comparison. The quadratic equation is fit to the 10 m resolution DEM data.
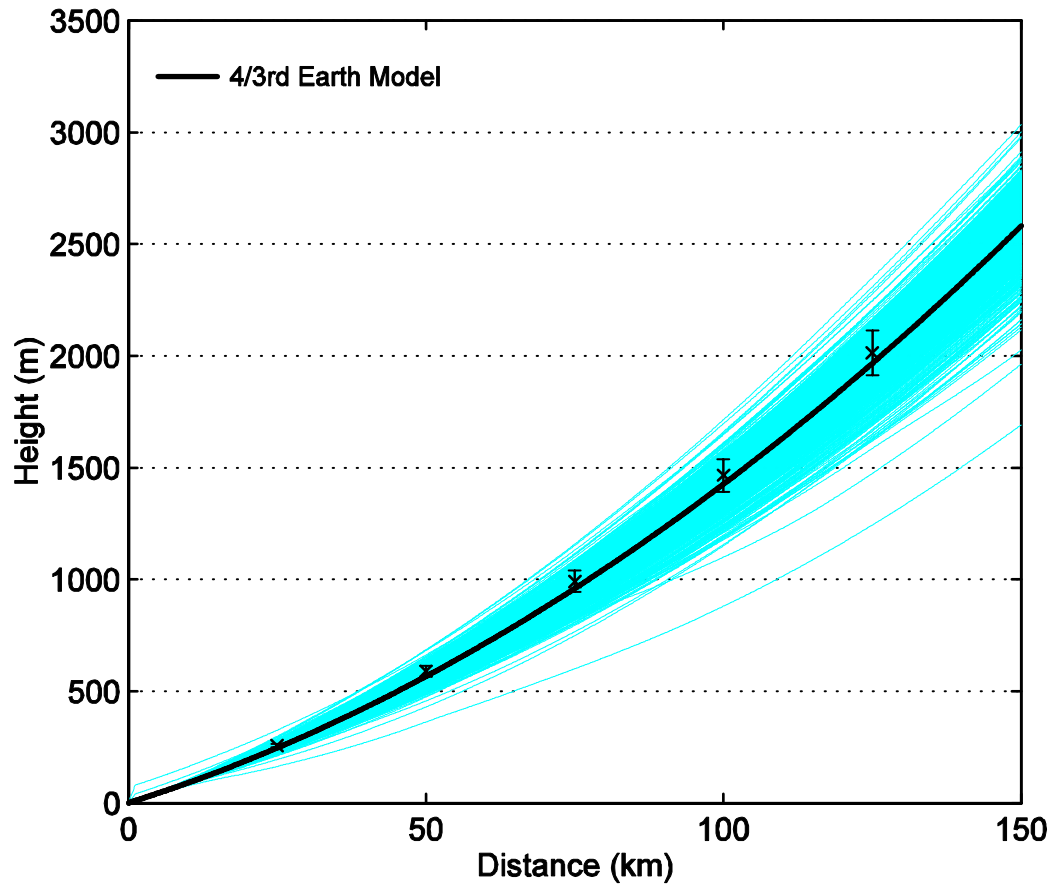
Figure 10: Beam height results using index of refraction derived from 2173 Guam soundings (Gray). The standard refractive index beam height (4/3rd Earth) is shown as the solid black line. The symbols indicate the mean calculated height and the vertical bars show +/- 1 standard deviation about the mean at ranges of 25, 50, 75, 100, and 125 km, respectively.
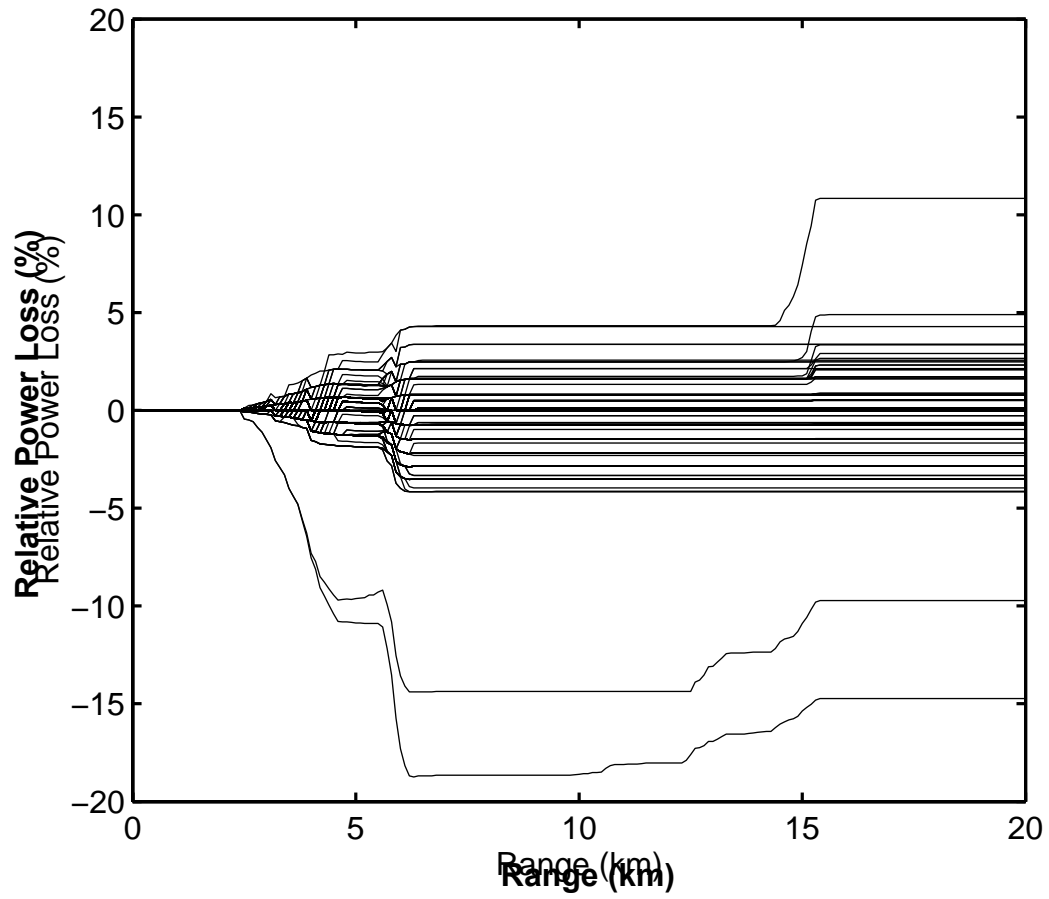
Figure 11: Relative power loss obtained from the ray propagation model and DEM data over the AAFB rain gauge site using the estimated beam heights given in Figure 10. The estimated power loss is compared to the power loss using the 4/3rd Earth approximation.
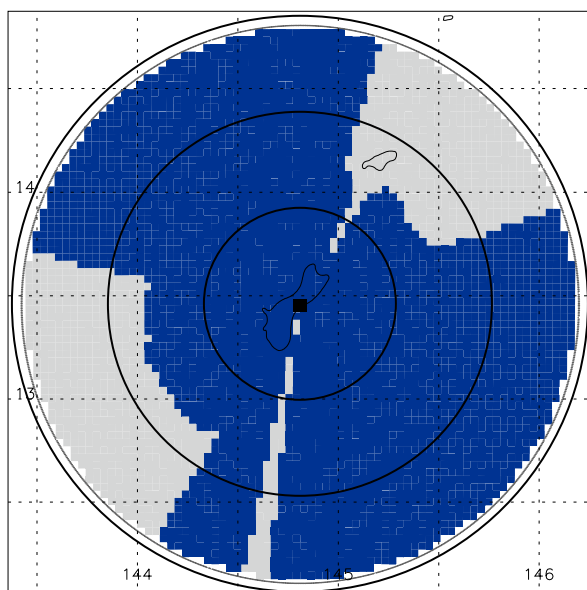
Figure 12: Guam product map with 50 km range rings (approximately). Regions masked in dark gray are considered valid. Regions in light gray are marked as bad and not used in radar-rainfall analysis.